

Raman scattering in $\text{YBa}_2\text{Cu}_3\text{O}_7$: A comprehensive theoretical study in comparison with experiments

C. Ambrosch-Draxl, H. Auer, R. Kouba, and E. Ya. Sherman
Institute of Theoretical Physics, Karl-Franzens-University of Graz, A-8010 Graz, Austria

P. Knoll and M. Mayer
Institute for Experimental Physics, Karl-Franzens-University of Graz, A-8010 Graz, Austria

(Received 10 July 2001; published 3 January 2002)

All Raman-active phonon modes of $\text{YBa}_2\text{Cu}_3\text{O}_7$ are investigated by first-principles linearized augmented plane-wave calculations based on density-functional theory for a fully optimized crystal structure. The calculated frequencies as well as the Raman scattering intensities are in excellent agreement with measured Raman spectra. The effect of site-selective isotope substitution on the Raman spectra is investigated. The substitution not only shifts the phonon frequencies, but also leads to dramatic changes in the scattering intensities.

DOI: 10.1103/PhysRevB.65.064501

PACS number(s): 74.25.Kc, 74.25.Jb, 78.30.-j, 71.15.Mb

I. INTRODUCTION

The electronic properties of high- T_c superconducting cuprates are strongly governed by their crystal structure. Displacements of ions from their equilibrium positions as caused by vibrational modes lead to changes in the electronic structure, due to strong electron-phonon coupling in these compounds. Electron-phonon coupling and the role of the lattice were subject of investigation since the discovery of high- T_c superconductivity. Results of these investigations indicate the importance of the coupling of electrons to the lattice in the normal state as well as a significant relation between phonons and the superconducting transition.

When ions are displaced from their equilibrium positions, the increase of the total energy leads to lattice forces which push them back and thereby result in lattice vibrations. At the same time the crystal's electronic structure and the related properties are changed. When an electromagnetic wave propagates through a crystal, its frequency is changed due to the modulation of the dielectric tensor caused by the time-dependent ionic displacements. This light scattering by lattice vibrations results in the Raman process.

Since Raman scattering is determined by the influence of the ionic motions on the electronic states in a wide energy range, Raman spectroscopy provides valuable information on both, the lattice properties as well as the electronic subsystem. The total energy and the dielectric tensor as a function of the atomic coordinates required for the theoretical description of the Raman spectra can be obtained by first-principles band-structure methods within the frozen-phonon approach. The total energy and the atomic forces acting on the displaced ions yield the force constants necessary to determine phonon frequencies and eigenvectors, while also the dependence of the dielectric tensor is used to calculate the Raman intensities.

First-principles calculations appeared to be very useful for describing the properties of high- T_c cuprates close to optimal doping, where they demonstrate good metallic behavior. While the Raman spectra of $\text{YBa}_2\text{Cu}_3\text{O}_{7-x}$ have been measured on some underdoped samples,^{1,2} the corresponding the-

oretical investigations are still lacking. This is due to the fact that first-principles calculations require an ordered structure which would lead to huge supercells for arbitrary doping levels. In this paper we focus on $\text{YBa}_2\text{Cu}_3\text{O}_7$ which is best studied, experimentally as well as theoretically.

It turned out that best agreement with experimental data is achieved when the crystal structure is optimized theoretically, i.e., when unit-cell volume, axis ratios, and atomic positions are obtained by searching for the lowest total energy.³ In order to study vibrational properties and phonon Raman scattering we have performed frozen-phonon calculations within this optimized crystal structure. We focus our attention on the Raman-active modes (zero-momentum transfer) which are divided into three symmetry classes: A_{1g} , B_{2g} , and B_{3g} . Each class contains five eigenmodes which are coupled vibrations of Ba, the plane copper atom Cu2, the plane oxygens O2 and O3, and the apical oxygen O4. The A_{1g} modes represent c -axis vibrations of these five atoms, while within the B_{2g} , and B_{3g} modes these atoms move in the a and b direction, respectively. The spectral densities of inelastic light scattering are quantitatively compared to measured spectra. Our approach also gives us the possibility to consider the site-selective isotope substitution and its influence on the phonon frequencies and scattering intensities.

II. METHOD

A. Raman scattering in the frozen-phonon approximation

In Raman spectroscopy a light beam with frequency ω_{rmi} irradiates a crystal, where the spectrum of scattered light is investigated. The spectrum of scattered light contains peaks around the frequencies $\omega_S = \omega_I - \omega_{ph}$ (Stokes process) and $\omega_S = \omega_I + \omega_{ph}$ (anti-Stokes process), where ω_{ph} is a phonon frequency. To calculate the scattering probability, first the frequencies and eigenvectors of the zero-momentum phonons are determined by solving the eigenvalue equation

$$\hat{D}\mathbf{Q}_\zeta = \omega_\zeta^2 \mathbf{Q}_\zeta. \quad (2.1)$$

Here $\mathbf{Q}_\zeta = (\mathbf{e}_{1\zeta}, \dots, \mathbf{e}_{\alpha\zeta}, \dots, \mathbf{e}_{N\zeta})$ is the eigenvector of the phonon mode ζ with frequency ω_ζ , which, in general consists of $3N$ components, where N is the number of atoms per unit cell. Index $\alpha = 1, \dots, N$ numerates the ions, and $\mathbf{e}_{\alpha\zeta}$ is the displacement of the ion. The elements of the dynamical matrix \hat{D} are the mass-weighted force constants $F_{ij}^{\alpha\beta}$,

$$D_{j,l}^{\alpha,\beta} = \frac{F_{jl}^{\alpha\beta}}{\sqrt{M_\alpha M_\beta}} = \frac{1}{\sqrt{M_\alpha M_\beta}} \frac{\partial^2 E_{tot}}{\partial u_j^\alpha \partial u_l^\beta}, \quad (2.2)$$

where E_{tot} is the total energy of the system as a function of ionic displacements u_j^α , M_α is the mass of atom α , and $j, l = x, y, z$ are Cartesian indices. Generally, they couple all $3N$ degrees of freedom, since the displacement of atom α in direction j can result in a force acting on atom β in direction l . However, the dynamical matrix \hat{D} is usually split in smaller blocks determined by the crystal symmetry, allowing a simpler treatment of the problem. As a result, some components of the vector \mathbf{Q}_ζ vanish. For $\text{YBa}_2\text{Cu}_3\text{O}_7$, each of the classes— A_{1g} , B_{2g} , and B_{3g} —is represented by a 5×5 block of the dynamical matrix. The atomic displacements in a given mode are expressed by

$$\mathbf{u}_\zeta^\alpha = \text{const} \frac{\mathbf{e}_{\alpha\zeta}}{\sqrt{M_\alpha}}. \quad (2.3)$$

Within the frozen-phonon approximation, the atomic displacements are treated as a quasistatic perturbation, which influences the electron band energies and wave functions, and increases the crystal's total energy. After calculating the total energies for different displacement patterns the energy surface can be expanded as a polynomial in all displacement coordinates,

$$E_{tot} = A_0 + \sum_{j,\alpha} A_j u_j^\alpha + \frac{1}{2} \sum_{j,\alpha} \sum_{l,\beta} A_{jl} u_j^\alpha u_l^\beta + \frac{1}{6} \sum_{j,\alpha} \sum_{l,\beta} \sum_{m,\gamma} A_{jlm} u_j^\alpha u_l^\beta u_m^\gamma + \dots, \quad (2.4)$$

where the coefficients are obtained by a fitting procedure. The numerical effort is dramatically reduced if not only the total energy is computed self-consistently, but also the forces acting on the atoms within the unit cell. In this case, the coefficients can be determined by fitting the atomic forces, where the number of configurations needed scales linearly in N . This procedure not only improves the accuracy of the results by providing more data for the same number of configurations, but makes the investigations of complex systems like high- T_c materials feasible.⁴ From the energy surface the force constants are computed, where the phonon frequencies ω_ζ and eigenvectors \mathbf{Q}_ζ are obtained by diagonalizing the dynamical matrix, i.e., solving Eq. (2.1). After diagonalization, the energy can be written as a one-dimensional potential as a function of each phonon eigenvector,

$$E_{tot} = a_0 + a_2 Q_\zeta^2 + \dots, \quad (2.5)$$

with the frequency of the mode determined by the coefficient a_2 . A theoretical analysis of phononic Raman intensities in crystals has been given by several authors.⁵⁻⁷ In this paper, we follow the description of the Raman scattering process derived with the aim to calculate Raman spectra from observables which can be directly obtained from frozen-phonon *ab initio* band-structure calculations.^{8,9} The quantum-mechanical expression for the Raman efficiency caused by the transitions between the eigenstates $|i\rangle$ and $|f\rangle$ with energies E_f and E_i , respectively, is given by⁸

$$S_{jl}^{i \rightarrow f} = \frac{N_\Omega \Omega \omega_l \omega_s^3}{(4\pi)^2 c^4} |\delta \varepsilon_{jl}^{i \rightarrow f}|^2, \quad (2.6)$$

where $N_\Omega \Omega$ is the coherence volume with Ω being the volume of the elementary cell, and c is the velocity of light. j and l denote the polarization direction of the incident and scattered light, respectively. Here we restrict our considerations to one-phonon scattering, while the higher-order perturbation processes are described in the Appendix. The matrix element of the transition arising due to fluctuations of the dielectric function in a phonon mode Q_ζ has the form

$$\begin{aligned} \delta \varepsilon_{jl}^{i \rightarrow f} &= \langle f | \delta \hat{\varepsilon}_{jl}^{\omega_l} | i \rangle = \langle f | \frac{\partial \varepsilon_{jl}^{\omega_l}}{\partial Q_\zeta} \hat{Q}_\zeta | i \rangle \\ &= \frac{\partial \varepsilon_{jl}^{\omega_l}}{\partial Q_\zeta} \langle \nu | \hat{Q}_\zeta | \mu \rangle \equiv \delta \varepsilon_{jl}^{\mu \rightarrow \nu}. \end{aligned} \quad (2.7)$$

Here we have made use of the adiabatic approximation, i.e., writing the eigenstates of the many-body system as a product $|\mu\rangle \otimes |g\rangle$ of vibrational states $|\mu\rangle$ and electronic states $|g\rangle$, where the latter are independent of Q_ζ . Thus the transition between the eigenstates occurs in the phononic subsystem only with $|i\rangle \rightarrow |f\rangle = |\mu\rangle \otimes |g\rangle \rightarrow |\nu\rangle \otimes |g\rangle$. In this case the matrix element in Eq. (2.7) is a product of an electronic and a phononic contribution, which can be evaluated separately. The total Raman efficiency of one phonon mode at temperature T is given by the thermal average over the contributions of all possible transitions:

$$S_{jl} = \frac{N_\Omega \Omega \omega_l \omega_s^3 \sum_\mu e^{-E_\mu/kT} \sum_\nu [\delta \varepsilon_{jl}^{\mu \rightarrow \nu}]^2}{(4\pi)^2 c^4 \sum_\mu e^{-E_\mu/kT}}. \quad (2.8)$$

This expression describes the integrated line intensity of the observed Raman spectrum. For direct comparison with experiment the spectral density as a function of the Raman shift $\omega_R = \omega_l - \omega_s$ can be obtained by introducing a normalized line shape L in account for phonon lifetimes:

$$\sigma_{jl}(\omega_R) = \frac{N_\Omega \Omega (\omega_I - \omega_R)^3 \sum_\mu e^{-E_\mu/kT} \sum_\nu [\delta \varepsilon_{jl}^{\mu \rightarrow \nu}]^2 L(\omega_R, \omega_{\mu\nu}, \Gamma)}{(4\pi)^2 c^4 \sum_\mu e^{-E_\mu/kT}}, \quad (2.9)$$

where Γ is the phonon linewidth, and $\omega_{\mu\nu}$ is the phonon frequency. For $L(\omega_R, \omega_{\mu\nu}, \Gamma)$, usually a Lorentzian shape is taken.

Like the phonon potential in Eq. (2.5), the frequency dependent dielectric tensor can be expanded as a polynomial in terms of the phonon eigenvector with the coefficients being obtained by fitting to the first-principles results:

$$\varepsilon_{jl}(\omega) = b_0^{jl}(\omega) + b_1^{jl}(\omega) Q_\zeta + b_2^{jl}(\omega) Q_\zeta^2 + \dots \quad (2.10)$$

In this case the derivatives of the dielectric functions appearing in Eq. (2.7) are represented by the coefficients of the polynomial at the incident photon energy. The pure vibronic matrix elements are calculated numerically after solving the harmonic (or anharmonic) oscillator problem for the potential given in Eq. (2.4). The expressions (2.5) and (2.10) thus contain all the information necessary from the band-structure calculations to determine the Raman spectra for a certain eigenmode. One can see from Eq. (2.7) that the eigenvectors of the vibrations are crucially important for the Raman scattering intensities, and therefore precise knowledge of all relevant force constants is needed to reliably describe the Raman spectra.

B. Computational details

The calculations, which are based on density-functional theory (DFT), are carried out within the full-potential linearized augmented plane-wave (LAPW) method¹⁰ using the program package WIEN97.¹¹ Exchange and correlation effects are treated within the local-density approximation (LDA). In order to account for overbinding effects by LDA we fully relaxed the crystal structure,³ i.e., lattice parameters as well as atomic positions. Thereby the volume turned out to be 6% smaller than the experimental one. The so obtained geometry was the starting point for the frozen phonon calculations to determine frequencies and eigenmodes of all 15 Raman-active phonons and the scattering intensities for the 5 A_{1g} vibrations.

Our basis set includes approximately 2000 basis functions supplemented by local orbitals for the treatment of semicore states $Y-4s$, $Y-4p$, $Ba-5s$, $Ba-5p$, $Ba-4d$, $Cu-3s$, $Cu-3p$, $O-2s$. For the A_{1g} modes the Brillouin-zone integrations were carried out on a \mathbf{k} -point mesh consisting of 243 points in the irreducible wedge (IBZ) using a Gaussian smearing of 0.002 mRyd. For the B_{2g} and B_{3g} vibrations 144 \mathbf{k} points in the IBZ turned out to give sufficient accuracy. In all cases, the \mathbf{k} -point mesh was further increased for the computation of the dielectric tensors. The details of the optimization procedure can be found in Ref. 3.

The force constants were established by least-square fits of atomic-force values calculated for 8 to 13 different distortion patterns for each class of modes (the actual number depending on the symmetry). After diagonalization of the dynamical matrix the atoms were again displaced along the eigenvector. Thereby we could cross check the accuracy of the fitting procedure and, more important, accurately describe the dielectric tensor as a function of displacement according to the exact normal coordinate as given in Eq. (2.10).

III. RESULTS AND DISCUSSION

A. Phonon frequencies and eigenvectors

Table I shows the phonon frequencies and the corresponding eigenvectors of all the Raman-active modes obtained by solving Eq. (2.1). Although the A_{1g} data have been published elsewhere³ they are repeated for completeness and further comparison to the results for site-selective isotope substitution. All phonon frequencies excellently reproduce their experimental counterparts, with a significant improvement achieved compared to the calculations carried out for the experimental structural parameters.^{4,18,19} The corresponding eigenvectors generally reflect the fact that the motion of one atom is now less influenced by the displacement of the other atoms. This was pointed out already in Ref. 3 for the A_{1g} modes. In particular, it should be mentioned that the O4 contribution to the O2–O3 mode is much smaller in comparison to the result obtained with experimental lattice parameters, since this admixture is responsible for dramatic effects on the Raman-scattering intensity as will be shown below. It should also be mentioned that the eigenvectors are in good agreement to those estimated from experimental data.²² For the B_{2g} and B_{3g} vibrations, the modes are clearly dominated by one atomic species. Note that O2 (O3) in the B_{2g} (B_{3g}) mode has a large vibrational frequency due to the stretching of a rigid Cu–O2 (Cu2–O3) bond in $x(y)$ direction.

In addition to already published experimental data, micro-Raman measurements have been performed on single crystals at room temperature using the scanning multichannel technology.²⁰ From the different polarization geometries the phonon frequencies have been determined for the different symmetry species as given in Table I. In contrast to the data available in literature, the frequencies of the totally symmetric modes have been taken in (zz) polarization. Due to the absence of interference of the phonons with the electronic background in this geometry we could determine the bare frequencies, which are 123, 152, 442, and 500 cm^{-1} . Only the out-of-phase oxygen vibration (often denoted as the B_{1g} mode) at 338 cm^{-1} has been measured in the usual 45° rotated ($x'y'$) cross polarization in the (xy) plane because

TABLE I. Phonon frequencies (in cm^{-1}) and eigenvectors for the A_{1g} , B_{2g} , and B_{3g} modes at $q=0$ in comparison to experimental data (this work and Refs. 12–17).

	Mode	ω_{exp}	ω_{th}	Ba	Cu2	O2	O3	O4
A_{1g} ($\parallel c$)	Ba	116-123	123	0.91	0.41	0.05	0.05	0.04
	Cu2	145-152	147	0.42	-0.90	-0.08	-0.06	0.00
	O2-O3	335-338	338	0.00	0.03	-0.77	0.63	-0.01
	O2+O3	435-442	422	0.03	0.11	-0.60	-0.73	-0.31
	O4	493-500	487	0.02	-0.02	0.19	0.24	-0.95
B_{2g} ($\parallel a$)	Ba	69-79	65	0.90	0.29	0.14	0.08	0.29
	Cu2	140-142	142	-0.35	0.82	0.38	0.24	0.00
	O4	209-210	222	-0.27	-0.09	-0.03	-0.04	0.96
	O3	370	389	0.00	-0.30	0.06	0.95	0.02
	O2	579-585	593	0.00	0.37	-0.91	0.18	0.02
B_{3g} ($\parallel b$)	Ba	78-83	79	0.91	0.32	0.10	0.15	0.18
	Cu2	140-141	141	-0.36	0.81	0.25	0.37	-0.03
	O4	303-307	293	-0.17	-0.04	-0.03	0.01	0.98
	O2	378	372	0.00	0.34	-0.93	-0.11	-0.01
	O3	526	546	0.00	-0.34	-0.23	0.90	-0.03

of its extremely small intensity in (zz) polarization. The absolute cross sections have been determined by accounting for absorbance, reflection, and refraction. The A_{1g} spectra are given in Fig. 2. The measured B_{3g} spectra clearly show the O2 mode at 378 cm^{-1} , which is excellently reproduced by our calculations.

B. Raman intensities

The calculated spectral densities are shown in Fig. 1 for diagonal scattering geometries at room temperature. For the Lorentzian line shapes an overall line broadening of $\Gamma = 35 \text{ K}$ has been chosen. Theory quantitatively reproduces the experimentally measured intensities presented in Fig. 2. For comparison, in Fig. 1 the calculated intensity of the Ba and Cu mode are displayed (gray lines) when a smaller broadening of 18 K is used for the two low-energy modes. With this choice, for the (zz) polarization not only the integrated intensities, but also the spectral densities excellently agree with their experimental counterparts. The intensities of the in-plane polarizations are more than one order of magnitude smaller than those in (zz) geometry as already found by Heyen *et al.*²¹ in the resonant Raman scattering.

The resonant behavior of the total efficiency $S_{zz}(\omega)$ (that is the integrated spectral density) is presented in Fig. 3. Since Raman-scattering experiments exhibit the phonon frequencies but at the same time probe the components of normal vectors, the Raman intensities contain much information about the precision of the calculated eigenvectors. The displacement of the apical oxygen has the strongest effect on the electronic structure and thus gives rise to the biggest scattering intensity^{21,23} among the A_{1g} modes in (zz) polarization. Since $\partial \epsilon_{zz}(\omega)/\partial u_{O4}$, i.e., the change of the dielectric function with O4 displacement, is large, the contribution of the apical oxygen plays an important role for the Raman

intensity of both the O4 and O2+O3 modes. The dependence of $\epsilon_{zz}(\omega)$ upon displacements of the atoms with respect to the eigenvectors of these two modes is seen in Figs. 4 and 5. The strong change with the O4 coordinate (eigenvector) arises due to the large z -coordinate matrix element between the $O4(p_z)$ and $Cu1(d_{z^2-y^2})$ orbitals contributing

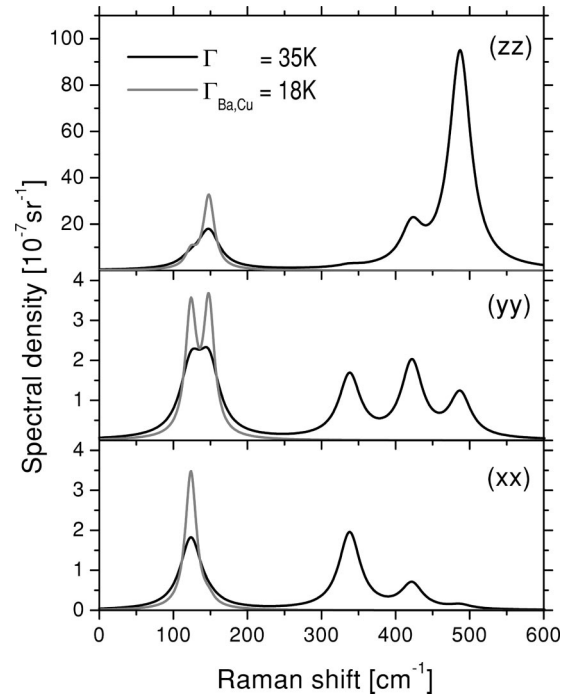


FIG. 1. Calculated Raman intensities (black lines) of the A_{1g} modes for a laser wavelength of 514 nm in (xx), (yy), and (zz) polarization at room temperature. An overall lifetime broadening of $\Gamma = 35 \text{ K}$ was used. For comparison, the grey curves show the corresponding spectra for the Ba and Cu mode, when $\Gamma = 18 \text{ K}$.

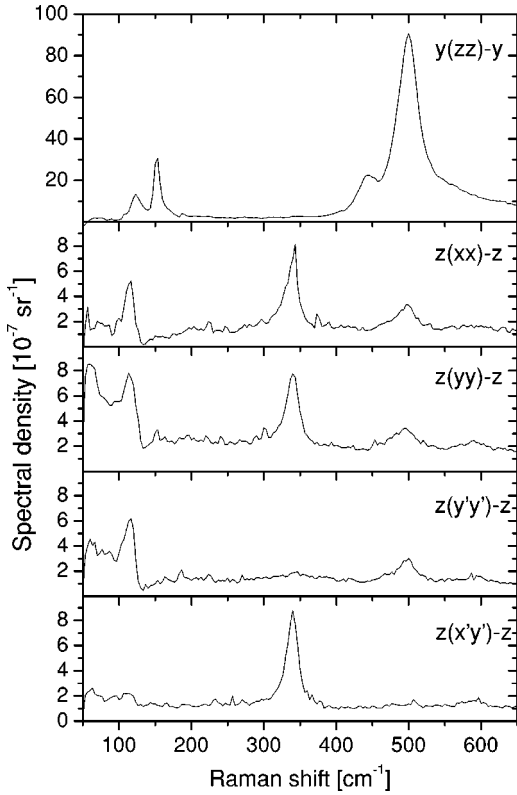


FIG. 2. Measured Raman intensities in different geometries for a laser wavelength of 514 nm at room temperature. The A_{1g} frequencies are determined to be 123, 152, 338, 442, and 500 cm^{-1} , respectively.

to $\epsilon_{zz}(\omega)$. Due to a resonance of the incident light with the interband transition between the bands where these orbitals are heavily involved, $\epsilon_{zz}(\omega)$ is strongly modulated by the ion displacement. For the in-plane states this matrix element arises only due to the small buckling of the CuO_2 layers, being weakly modulated by the displacements of plane oxygen ions. For that reason the plane oxygen ions give a relatively small contribution to the Raman activity in (zz) polarization.

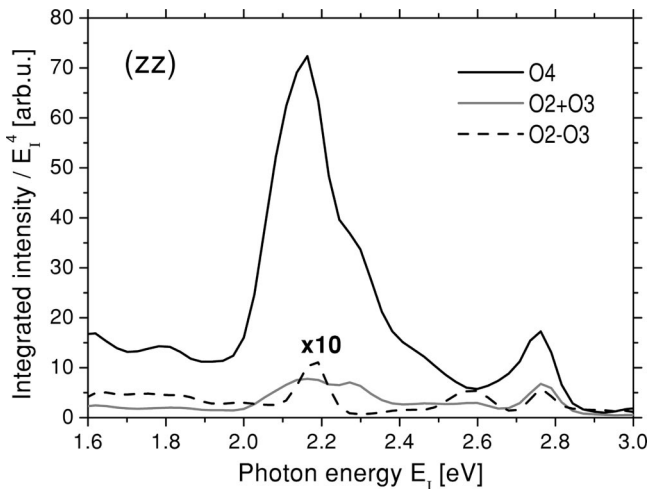


FIG. 3. Resonance behavior of the Raman intensity in (zz) polarization for the three oxygen dominated modes.

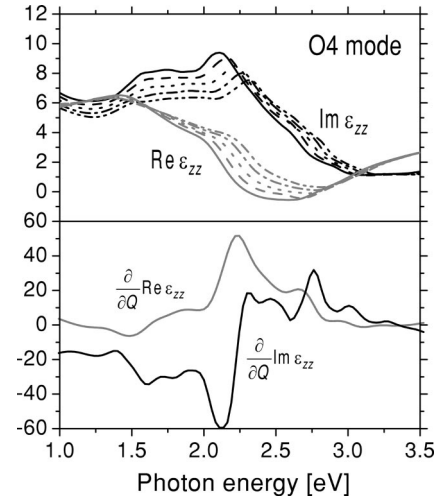


FIG. 4. Real and imaginary part of the dielectric tensor component ϵ_{zz} for different atomic displacements along the eigenvector of the O4 mode (upper panel). The lines correspond to the O4 ion displacement of 0.025 Å (solid), 0.0125 Å (dashed), 0 (dotted), -0.0125 Å (dash-dotted), and -0.025 Å (double dash-dotted). In addition the corresponding derivatives are displayed (lower panel).

Previously, a good overall agreement between theory and experiment of the Raman intensities as a function of ω_1 was found. The only exception was the O2–O3 mode in (zz) polarization where a much too high intensity was obtained by the linear muffin-tin orbital (LMTO) calculations.²¹ This behavior can be understood by the large contribution of the O4 displacement in the normal vector used in Ref. 21. As can be seen in Figs. 1 and 3 this discrepancy is lifted when taking into account the eigenvector displayed in Table I. In excellent agreement with experiment^{21,22} the intensity of the O4 mode at the peak position is approximately seven times as big as for the O2+O3 mode, whereas the Raman efficiency of the O2–O3 mode is two orders of magnitude smaller than that of the O4 vibration.

During the vibrations of B_{2g} and B_{3g} symmetry, the atoms are displaced from positions lying in a mirror plane. The displacement to both directions is equivalent leading to a symmetric potential and a saddle point in the dielectric function ϵ_{jj} . For the latter reason, the first derivative of this quantity and hence the Raman intensity in diagonal polariza-

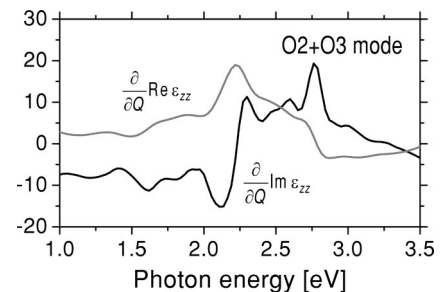


FIG. 5. Derivatives of real and imaginary part of the dielectric tensor component ϵ_{zz} with respect to the eigenvector of the O2+O3 mode.

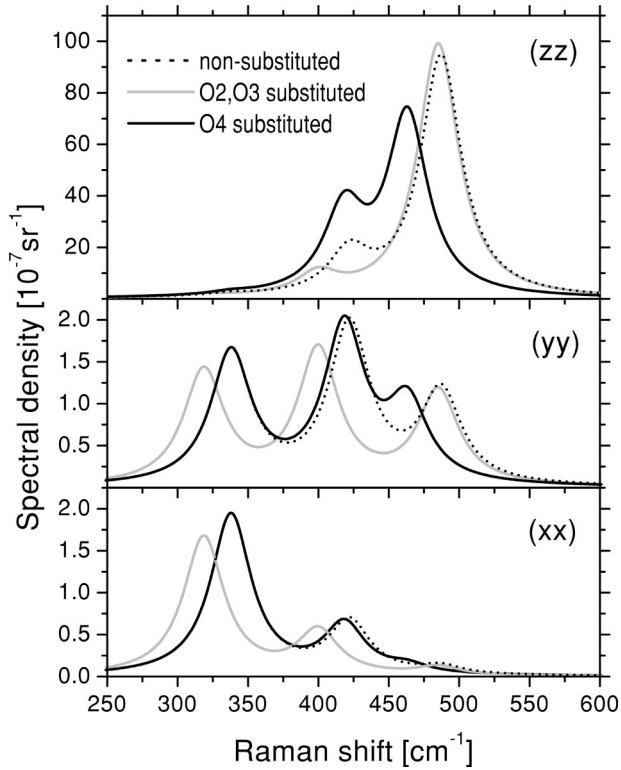


FIG. 6. Isotope effect on the Raman spectra of the three oxygen modes in (xx) , (yy) , and (zz) polarization. The grey (black) lines indicate substitution of the plane (apex) oxygen atoms by ^{18}O , whereas the dashed lines correspond to the case without substitution.

tions is zero. Due to the lowering of the symmetry finite nondiagonal terms are allowed, but they are very small. Indeed, the measured Raman intensities are two orders of magnitude smaller than those of the A_{1g} modes. This finding is also reproduced by our calculations.

C. Site-selective isotope effect in Raman spectra

Technologically, it is possible to produce the $\text{YBa}_2\text{Cu}_3\text{O}_7$ crystals with a site-selective oxygen isotope substitution, i.e.,

where only the plane or the apical oxygen sites are occupied by another isotope.^{24–28} Thereby the influence on T_c strongly depends on the type of the substitution. Replacement of oxygen atoms by their ^{18}O isotopes has two effects on the Raman spectra. First, the vibrational frequencies are lowered due to the increased ionic mass. Second, the phonon eigenvectors are altered as well. As already mentioned above, the Raman intensities strongly depend on the eigenvector of a mode, and therefore modifications in the eigenvectors directly cause changes in the phonon intensities.²⁹ In contrast, a substitution of all oxygens by isotopes, only cause a frequency decrease of the oxygen modes by $\sqrt{16/18}$ and does not affect the eigenvectors, since the oxygen modes can be regarded to be decoupled from the Ba-Cu subsystem.

Figure 6 presents the Raman intensities for two different cases of the $^{16}\text{O} \rightarrow ^{18}\text{O}$ substitution compared to the results for the nonsubstituted crystal. The eigenvectors and frequencies are represented in Tables II and III, respectively. The dramatic effects of the site-selective substitution on the intensities of the O2+O3 mode and the O4 mode can be understood in the following way. In the nonsubstituted crystals these modes are close in frequency and hence considerably mixed.²² In the case of $^{18}\text{O}_4$ ($^{18}\text{O}_2, ^{18}\text{O}_3$) substitution the modes become more (less) close in frequency, and therefore the vibrations of the atoms involved get more (less) strongly coupled. This fact leads to changes in the Raman intensities as shown in Fig. 6 and their resonant behavior.

Excellent agreement between theory and experiment is found for the frequency shifts (see Tables II and III) where experimental data are available.²⁵ The relatively small deviations from the measured values can be understood by the uncertainties in the substitution: For the O4 substituted samples a 15% replacement of the plane oxygens was estimated. Since the O4 mode is nearly completely decoupled from the plane atoms, the additional replacement of plane oxygens does not affect the O4 frequency. In this case, the experimental frequency shift is in perfect agreement with theory. In contrast, the shift of the experimental O2+O3 frequency is enhanced by the ^{18}O content of the planes. The same holds for the O2–O3 mode, where a small frequency

TABLE II. Phonon frequencies and frequency shifts (in cm^{-1}), and eigenvectors for the oxygen modes in A_{1g} , B_{2g} , and B_{3g} symmetries for plane oxygen isotope substitution. Experimental data are taken from Ref. 25.

Symmetry	Mode	ω	$\Delta\omega$	$\Delta\omega_{exp}$	Ba	Cu2	O2	O3	O4
A_{1g}	O2–O3	318.5	–19.3	–17	0.01	–0.03	0.77	–0.63	–0.01
	O2+O3	399.7	–22.2	–21	0.03	0.12	–0.61	–0.75	–0.21
	O4	485.0	–2.0		–0.03	0.01	–0.14	–0.19	0.97
B_{2g}	O4	222.4	0.0		0.27	0.09	0.03	0.05	–0.96
	O3	368.6	–20.2		0.00	–0.30	0.04	0.95	0.02
	O2	564.3	–29.0		0.00	–0.38	0.91	–0.17	–0.02
B_{3g}	O4	292.9	0.0		–0.18	–0.03	–0.04	0.01	0.98
	O2	353.5	–18.7		0.00	–0.34	0.94	0.08	0.02
	O3	518.6	–27.3		0.00	–0.35	–0.22	0.91	–0.03

TABLE III. Phonon frequencies and frequency shifts (in cm⁻¹), and eigenvectors for the oxygen modes in A_{1g} , B_{2g} , and B_{3g} symmetries for apical oxygen isotope substitution. Experimental data are taken from Ref. 25.

Symmetry	Mode	ω	$\Delta\omega$	$\Delta\omega_{exp}$	Ba	Cu2	O2	O3	O4
A_{1g}	O2-O3	337.8	0.0		-0.01	0.03	-0.78	0.63	0.01
	O2+O3	418.3	-3.6	-8	0.04	0.11	-0.55	-0.67	-0.49
	O4	463.1	-23.9	-24	0.02	-0.03	0.28	0.35	-0.90
B_{2g}	O4	210.8	-11.6		0.27	0.09	0.03	0.04	-0.96
	O3	388.8	0.0		0.00	-0.30	0.06	0.95	0.02
	O2	593.3	0.0		0.00	-0.37	0.91	-0.18	-0.02
B_{3g}	O4	276.7	-16.2		0.18	0.03	0.02	-0.00	-0.98
	O2	372.2	0.0		0.00	-0.34	0.93	0.11	0.01
	O3	545.9	0.0		0.00	-0.34	-0.23	0.91	-0.03

shift can be seen in the spectrum, but no experimental value is given in Ref. 25. At the plane oxygen substitution only a 5% replacement of the apical and chain oxygen was determined. Therefore the effects can be estimated to be much smaller than in the case discussed above. The experimental scattering intensities also allow for a comparison with the calculated spectra to some extent, e.g., the relative increase of the O2+O3 mode with respect to the O4 mode, when ¹⁶O4 is replaced by ¹⁸O4, is well reproduced by our calculations. For a detailed analysis, however, more information from experimental side is needed.

Isotope substitution at the ¹³⁴Ba and ⁶⁵Cu sites shows only a minor influence on the intensities of corresponding phonons. This effect can be understood by the small mixing of these modes, clearly seen in Table I. The effect on phonon frequencies and eigenvectors of the Ba and Cu dominated modes in all three symmetry classes are shown in Tables IV and V. Comparison with experiments³⁰ for the A_{1g} modes as discussed in Ref. 9 demonstrates excellent agreement again confirming the precision of the calculated eigenvectors.

ACKNOWLEDGMENT

This work was supported by the Austrian Science Fund, projects P11893-PHY, P13430-PHY, and M591-TPH.

TABLE IV. Phonon frequencies and frequency shifts (in cm⁻¹), and eigenvectors for the barium and copper mode for A_{1g} , B_{2g} , and B_{3g} symmetries for barium isotope substitution. Experimental values taken from Ref. 30.

Symmetry	Mode	ω	$\Delta\omega$	$\Delta\omega_{exp}$	Ba	Cu2	O2	O3	O4
A_{1g}	Ba	124.4	-1.2	-1.3±0.2	0.89	0.44	0.05	0.05	0.04
	Cu	147.6	-0.3	-0.1±0.2	0.44	-0.89	-0.08	-0.05	-0.00
B_{2g}	Ba	65.8	-0.6		-0.89	-0.30	-0.14	-0.08	-0.29
	Cu	142.3	-0.2	0.0±0.5	0.35	-0.82	-0.38	-0.24	0.00
B_{3g}	Ba	80.0	-0.8		-0.91	-0.33	-0.10	-0.16	-0.18
	Cu	140.9	-0.2	-0.4±0.5	-0.37	0.81	0.25	0.37	-0.04

APPENDIX

By taking into account the higher-order terms in the \hat{Q} expansion of the dielectric function, we can write the matrix element for the transition between the states $|\mu\rangle$ and $|\nu\rangle$ in their general form (staying within the adiabatic approximation),

$$\delta\varepsilon_{jl}^{\mu\rightarrow\nu} \sim \sum_n \frac{1}{n!} \sum_{\zeta_n, \mathbf{q}_n} \frac{\partial^n \varepsilon_{jl}^{\omega_1}}{\partial Q_{\zeta_1 \mathbf{q}_1} \cdots \partial Q_{\zeta_n \mathbf{q}_n}} \times \langle \nu | \hat{Q}_{\zeta_1 \mathbf{q}_1} \cdots \hat{Q}_{\zeta_n \mathbf{q}_n} | \mu \rangle \quad (\text{A1})$$

which reduces to Eq. (2.7) when only one specific mode at $q=0$ is considered. Here $\hat{Q}_{\zeta_n, \mathbf{q}_n}$ is the eigenvector for the phonon branch ζ_n with momentum \mathbf{q}_n . Taking into account only one branch Eq. (A1) can further be split into one-, two-, three-phononic, contributions, etc., all of them with total momentum transfer $\mathbf{q}_1 + \mathbf{q}_2 + \cdots + \mathbf{q}_n = 0$ as needed for light scattering in solids:

TABLE V. Phonon frequencies and frequency shifts (in cm^{-1}), and eigenvectors for the barium and copper mode for A_{1g} , B_{2g} , and B_{3g} symmetries for copper isotope substitution. Experimental values taken from Ref. 30.

Symmetry	Mode	ω	$\Delta\omega$	$\Delta\omega_{exp}$	Ba	Cu2	O2	O3	O4
A_{1g}	Ba	122.9	-0.3	-0.2 ± 0.2	0.90	0.44	0.05	0.05	0.04
	Cu	145.9	-1.3	-2.1 ± 0.2	0.44	-0.90	-0.07	-0.05	-0.00
B_{2g}	Ba	65.1	-0.1		-0.90	-0.30	-0.14	-0.08	-0.29
	Cu	141.1	-1.1	-0.7 ± 0.5	0.35	-0.83	-0.38	-0.23	0.00
B_{3g}	Ba	79.1	-0.1		-0.91	-0.33	-0.10	-0.15	-0.18
	Cu	139.6	-1.0	-1.3 ± 0.5	-0.37	0.82	0.25	0.37	-0.03

$$\begin{aligned}
[\delta\epsilon_{jl}^{\mu \rightarrow \nu}]^{(1)} &= \frac{\partial \epsilon_{jl}^{\omega_1}}{\partial Q_0} \langle \nu | \hat{Q}_0 | \mu \rangle + \frac{1}{2} \frac{\partial^2 \epsilon_{jl}^{\omega_1}}{\partial Q_0^2} \langle \nu | \hat{Q}_0^2 | \mu \rangle + \frac{1}{6} \frac{\partial^3 \epsilon_{jl}^{\omega_1}}{\partial Q_0^3} \langle \nu | \hat{Q}_0^3 | \mu \rangle + \dots \\
[\delta\epsilon_{jl}^{\mu \rightarrow \nu}]^{(2)} &= \sum_{\mathbf{q} \neq 0} \left\{ \frac{1}{2} \frac{\partial^2 \epsilon_{jl}^{\omega_1}}{\partial Q_{\mathbf{q}} \partial Q_{-\mathbf{q}}} \langle \nu | \hat{Q}_{\mathbf{q}} \hat{Q}_{-\mathbf{q}} | \mu \rangle + \frac{1}{24} \frac{\partial^4 \epsilon_{jl}^{\omega_1}}{\partial Q_{\mathbf{q}}^2 \partial Q_{-\mathbf{q}}^2} \langle \nu | \hat{Q}_{\mathbf{q}}^2 \hat{Q}_{-\mathbf{q}}^2 | \mu \rangle + \dots \right\} \\
[\delta\epsilon_{jl}^{\mu \rightarrow \nu}]^{(3)} &= \sum_{\mathbf{q}, \mathbf{q}'} \left\{ \frac{1}{6} \frac{\partial^3 \epsilon_{jl}^{\omega_1}}{\partial Q_{\mathbf{q}} \partial Q_{\mathbf{q}'} \partial Q_{-\mathbf{q}-\mathbf{q}'}} \langle \nu | \hat{Q}_{\mathbf{q}} \hat{Q}_{\mathbf{q}'} \hat{Q}_{-\mathbf{q}-\mathbf{q}'} | \mu \rangle + \dots \right\} \dots
\end{aligned} \tag{A2}$$

Σ' indicates that the sum does not include the terms already considered in the lower-order processes. The total spectral density is the sum of different contributions, analogous to Eq. (2.9):

$$\sigma_{ji}(\omega_{\mathbf{R}}) = \frac{N_{\Omega} \Omega (\omega_1 - \omega)^3 \sum_{\mu} e^{-E_{\mu}/kT} \sum_{\nu} \sum_n [\delta\epsilon_{jl}^{\mu \rightarrow \nu}]_{\omega_S}^{(n)2} L^{(n)}(\omega_{\mathbf{R}}, \omega_{\mu\nu}, \Gamma)}{(4\pi)^2 c^4 \sum_{\mu} e^{-E_{\mu}/kT}}. \tag{A3}$$

- ¹E. Altendorf, X. K. Chen, J. C. Irwin, R. Liang, and W. N. Hardy, *Phys. Rev. B* **47**, 8140 (1993).
- ²N. Poulakis, D. Palles, E. Lirokapis, K. Conder, E. Kalids, and K. A. Müller, *Phys. Rev. B* **53**, R534 (1996).
- ³R. Kouba, C. Ambrosch-Draxl, and B. Zangger, *Phys. Rev. B* **60**, 9321 (1999).
- ⁴R. Kouba and C. Ambrosch-Draxl, *Phys. Rev. B* **56**, 14 766 (1997).
- ⁵M. Cardona, *Light Scattering in Solids II* (Springer, Berlin, 1981).
- ⁶J. Tang and S. C. Albrecht, in *Raman Spectroscopy*, edited by H. A. Suymanski (Plenum Press, New York, 1970), Vol. 2, p. 33.
- ⁷W. Hayes and R. Loudon, *Scattering of Light by Crystals* (Wiley, New York, 1978).
- ⁸P. Knoll and C. Ambrosch-Draxl, in *Proceedings of the International Workshop on Anharmonic Properties of High- T_c Cuprates*, edited by D. Mihailovich, G. Ruani, E. Kaldis, and K. A. Müller (World Scientific, Singapore, 1995), p. 220.
- ⁹C. Ambrosch-Draxl, R. Kouba, and P. Knoll, *Z. Phys. B: Condens. Matter* **104**, 687 (1997).
- ¹⁰O. K. Andersen, *Phys. Rev. B* **12**, 3060 (1975).
- ¹¹P. Blaha, K. Schwarz, and J. Luitz, *WIEN97, A Full Potential Linearized Augmented Plane Wave Package for Calculating Crystal Properties*, edited by Karlheinz Schwarz (Techn. Universität Wien, Austria, 1999), ISBN 3-9501031-0-4.
- ¹²T. Strach, T. Ruf, E. Schoenherr, and M. Cardona, *Phys. Rev. B* **51**, 16 460 (1995).
- ¹³G. Burns, F. H. Dacol, F. Holtzberg, and D. L. Kaiser, *Solid State Commun.* **66**, 217 (1988).
- ¹⁴B. Friedl, C. Thompson, E. Schönherr, and M. Cardona, *Solid State Commun.* **76**, 1107 (1990).
- ¹⁵R. Liu, C. Thomsen, W. Kress, M. Cardona, B. Gegenheimer, F. W. de Wette, J. Prade, A. D. Kulkarni, and U. Schröder, *Phys. Rev. B* **37**, 7971 (1988).
- ¹⁶V. G. Hadjiev, M. N. Iliev, C. Raptis, L. Kalev, and B. M. Wanklyn, *Physica C* **166**, 225 (1990).
- ¹⁷K. F. McCarty, J. Z. Liu, R. N. Shelton, and H. B. Radousky, *Phys. Rev. B* **41**, 8792 (1990).
- ¹⁸R. E. Cohen, W. E. Pickett, and H. Krakauer, *Phys. Rev. Lett.* **64**, 2575 (1990).
- ¹⁹C. O. Rodriguez, A. I. Liechtenstein, I. I. Mazin, O. Jepsen, O. K.

- Andersen, and M. Methfessel, *Phys. Rev. B* **42**, 2692 (1990).
- ²⁰P. Knoll, R. Singer, and W. Kiefer, *Appl. Spectrosc.* **44**, 776 (1990).
- ²¹E. T. Heyen, S. N. Rashkeev, I. I. Mazin, O. K. Andersen, R. Liu, M. Cardona, and O. Jepsen, *Phys. Rev. Lett.* **65**, 3048 (1990).
- ²²O. V. Misochko, E. I. Rashba, E. Ya. Sherman, and V. B. Timofeev, *Phys. Rep.* **194**, 387 (1990).
- ²³E. I. Rashba and E. Ya. Sherman, *Pis'ma Zh. Eksp. Teor. Fiz.* **47**, 404 (1988) [*JETP Lett.* **47**, 482 (1988)].
- ²⁴M. Cardona, R. Liu, C. Thomsen, W. Kress, E. Schönherr, M. Bauer, L. Genzel, and W. König, *Solid State Commun.* **67**, 789 (1988).
- ²⁵D. Zech, H. Keller, K. Conder, E. Kaldis, E. Liarokapis, N. Poulakakis, and K. A. Müller, *Nature (London)* **371**, 681 (1994).
- ²⁶J. H. Nickel, D. E. Morris, and J. W. Ager, *Phys. Rev. Lett.* **70**, 81 (1993).
- ²⁷V. B. Vykhodets, T. E. Kurennykh, V. A. Pavlov, and A. A. Fotiev, *Pis'ma Zh. Eksp. Teor. Fiz.* **58**, 421 (1993) [*JETP Lett.* **58**, 431 (1993)].
- ²⁸S. I. Bredikhin, A. A. Maksimov, B. C. H. Steele, and I. I. Tartakovskii, *Physica C* **196**, 112 (1992).
- ²⁹The importance of investigating the site-selective isotope substitution by Raman spectroscopy was mentioned in E. Altendorf, J. Chrzanowski, J. C. Irwin, and J. P. Frank, *Phys. Rev. B* **43**, 2771 (1991).
- ³⁰R. Henn, T. Strach, E. Schönherr, and M. Cardona, *Phys. Rev. B* **55**, 3285 (1997).